

Automatic Complementary Separation Pruning Toward Lightweight CNNs

David Levin

Faculty of Engineering, Bar-Ilan University
Ramat Gan, 5290002, Israel

david.levin2@live.biu.ac.il

Gonen Singer

Faculty of Engineering, Bar-Ilan University
Ramat Gan, 5290002, Israel

gonen.singer@biu.ac.il

Abstract

In this paper, we present Automatic Complementary Separation Pruning (ACSP), a novel and fully automated pruning method for convolutional neural networks. ACSP integrates the strengths of both structured pruning and activation-based pruning, enabling the efficient removal of entire components such as neurons and channels while leveraging activations to identify and retain the most relevant components. Our approach is designed specifically for supervised learning tasks, where we construct a graph space that encodes the separation capabilities of each component with respect to all class pairs. By employing complementary selection principles and utilizing a clustering algorithm, ACSP ensures that the selected components maintain diverse and complementary separation capabilities, reducing redundancy and maintaining high network performance. The method automatically determines the optimal subset of components in each layer, utilizing a knee-finding algorithm to select the minimal subset that preserves performance without requiring user-defined pruning volumes. Extensive experiments on multiple architectures, including VGG-16, ResNet-50, and MobileNet-V2, across datasets like CIFAR-10, CIFAR-100, and ImageNet-1K, demonstrate that ACSP achieves competitive accuracy compared to other methods while significantly reducing computational costs. This fully automated approach not only enhances scalability but also makes ACSP especially practical for real-world deployment by eliminating the need for manually defining the pruning volume.

1. Introduction

Convolutional neural networks (CNNs) have revolutionized deep learning, achieving remarkable success in applications like image classification, object detection, and image segmentation [13, 41, 46]. However, these models, with millions of parameters, are computationally intensive, making deployment on resource-constrained devices challenging [16]. To overcome this, model compression techniques

have become vital, reducing model complexity, computational demands, and memory use, and facilitating their application in real-world environments.

Among these compression techniques, pruning [14], decomposition [6], quantization [45], and knowledge distillation [21] are widely studied. Pruning, in particular, removes redundant components to create more efficient, sparse networks without significant performance loss. The aim is to reduce parameters while maintaining accuracy, leading to faster inference and lower storage requirements.

Pruning techniques can be broadly categorized into two approaches: structured and unstructured pruning [30]. Unstructured pruning involves removing individual weights from the network based on certain criteria, such as the magnitude of the weights. While this method can lead to highly sparse models, the irregularity of the resulting network structure often limits its ability to fully leverage modern hardware acceleration [16]. This limitation arises because current hardware is optimized for dense matrix operations, meaning that the random removal of weights doesn't result in significant improvements in speed or efficiency. In contrast, structured pruning focuses on removing entire components, such as filters, channels, or layers, thereby maintaining a regular structure that is more compatible with hardware optimizations [2]. This method allows for greater speedups, as it reduces not only the parameter count but also the computational overhead in a way that is better aligned with hardware constraints [39].

Another class of pruning techniques relies on network activations, often referred to as activation-based pruning. These methods prune components based on their activation during the forward pass, requiring access to the dataset on which the model was trained [3]. By analyzing the activations, the method identifies less important components, which can be removed without significantly degrading performance. The advantage of activation-based pruning is that it can offer more fine-grained decisions regarding which components contribute less to the overall network output. However, a key limitation of these approaches is the need for the dataset during the pruning process.

A common challenge in many pruning techniques, regardless of the specific method, is the need for the user to manually define the size or extent of the pruning. Typically, users must specify the percentage or volume of components to be pruned, which often results in a trial-and-error process to identify the optimal pruning level. This approach not only consumes considerable time but also requires repeated evaluations to strike the right balance between model size and performance [58]. Such manual tuning diminishes the practicality of pruning in real-world applications, where time and computational resources are limited, and it hinders the scalability of pruning methods for larger networks or diverse deployment environments [4]. The need for user input in defining the pruning volume makes it difficult to achieve optimal results in an automated and efficient manner.

In this paper, we introduce Automatic Complementary Separation Pruning (ACSP), a novel approach that fully automates neural network pruning. ACSP integrates both structured pruning and activation-based pruning, allowing the removal of entire components such as channels or neurons while utilizing activations to retain the most critical elements. A key concept of ACSP is its ability to select components based on their complementary capabilities, ensuring diversity and reducing redundancy in the pruned network. Unlike many conventional methods that often rely on manual user input to define the pruning volume, ACSP automatically selects the smallest and most diverse subset of components in each layer, aiming to minimize redundancy. The principle of selecting components based on complementary abilities, particularly through graph-based methods, ensures that the chosen subset contributes diverse, non-overlapping capabilities to the network. The graph-based approach avoids redundancy by selecting components from distinct regions within the graph space, ensuring that each chosen component not only performs well across tasks but also offers unique capabilities. Such complementary selection using graphs has been successfully applied in various domains, including feature selection and clustering methods [29, 42, 59]. By adopting this principle, ACSP balances efficiency with performance, enabling substantial reductions in model size without sacrificing accuracy.

The pruning process is conducted iteratively, layer by layer. For each layer, ACSP constructs a graph space based on activations, encoding the separation capability of each component with respect to all class pairs, making the method inherently suited to supervised learning tasks. To ensure complementary selection, ACSP selects components from different regions of the graph space, emphasizing diversity and complementary separation capabilities. This enables the network to maintain high performance while reducing the number of components in the neural architecture. ACSP’s automated selection process uses a clustering algorithm and a knee-finding technique, making it both efficient

and scalable, and therefore practical for real-world applications. In summary, the contributions of this paper can be summarized as follows:

- This paper presents Automatic Complementary Separation Pruning (ACSP), a novel method that automatically determines the optimal subset of components to prune without requiring manual intervention, overcoming the limitations of user-defined pruning volumes and reducing redundancy in neural networks.
- ACSP combines the strengths of structured pruning with activation-based pruning, ensuring the efficient removal of entire components like neurons or channels while selecting components with complementary separation capabilities. This approach maintains the most critical elements, resulting in models that are both computationally efficient and hardware-friendly.
- Extensive experiments demonstrate that ACSP achieves significant reductions in computational costs while maintaining or improving accuracy across various popular architectures and datasets, making it a scalable and practical solution for real-world deployment.

2. Related Works

Structured Pruning. Structured pruning methods focus on the removal of entire components, such as neurons, filters, or channels, creating a more streamlined and efficient network architecture that is optimized for hardware acceleration. One such method is SCOP (Scientific Control Pruning) [52], which identifies redundant structures by introducing a control group mechanism with knockoff features designed to resemble real feature maps but remain label-independent. During pruning, SCOP applies scaling factors to real and knockoff features, pruning components that rely more on knockoff features, thus minimizing the impact of irrelevant factors. Another method, SANP (Structural Alignment for Network Pruning) [11] retains alignment between the pruned and original network through partial regularization, guided by an Architecture Generator Network (AGN) that selects the optimal sub-network during training. By reducing the structural gap between the full and pruned models, SANP enhances pruning efficiency, improves hardware compatibility, and maintains high model performance. Similarly, Random Channel Pruning [32] offers a simplified approach to structured pruning by randomly selecting channels for removal. Despite its simplicity, random pruning performs comparably to more advanced techniques, particularly when paired with fine-tuning. This method effectively reduces network complexity while maintaining performance, providing a straightforward yet competitive alternative for achieving efficient neural network architectures. DepGraph (Dependency Graph) [9] introduces a dependency graph to model the dependencies between layers in neural networks, allowing for automatic group-level

structured pruning. The method ensures that structurally dependent parameters across layers are pruned simultaneously, preserving network integrity. By leveraging these dependencies, DepGraph prunes groups of parameters, maintaining performance while reducing computational costs.

Activation-Based Pruning. Activation-based pruning methods rely on network activations during the forward pass to identify less important components, which are then pruned. DCP (Discrimination-aware Channel Pruning) [61] adds discrimination-aware losses to intermediate layers to prune channels that lack discriminative power, using activations to evaluate each channel’s contribution to classification accuracy. By balancing reconstruction errors and these losses, it retains only the most valuable channels. A greedy algorithm then selects and optimizes the channels, compressing the model while preserving or enhancing performance. Another activation-based method is Network Slimming [38], which uses L1 regularization on batch normalization scaling factors, which control channel activations, to induce sparsity. Channels with small scaling factors (and thus lower activations) are pruned. After pruning, the model is fine-tuned to recover or improve accuracy. ThiNet [40] prunes entire filters from convolutional layers based on their contribution to the next layer’s activations. Instead of using current-layer information, it evaluates next-layer activations to guide pruning. This pruning method reduces model size while retaining the original structure.

3. Method

3.1. Notation

Before introducing our method, we first describe the notations used throughout this paper. Let $F(D; W)$ denote a neural network, where D is the dataset and W represents the weights. We consider a dataset $D = (X, Y)$, with input data X and labels Y , where Y has C unique classes.

For a given network, let L_i represent the i -th layer with weights W_i . The number of components (such as neurons in a linear layer or channels in a convolutional layer) in layer L_i is denoted by N_i . The activations of layer L_i are marked as A_i . Let $\mathcal{I}_i = \{1, 2, \dots, N_i\}$ represent the set of indices for the components in layer L_i , with \mathcal{I}_i, j denoting the j -th component. For a convolutional layer, the activation $A_{i,j}[t]$, the output of the j -th component, is an activation map of size $p \times p$, for the t -th sample, where p represents the spatial dimensions. For a linear layer, $p = 1$, making $A_{i,j}[t]$ a scalar. The pruning process aims to find, for each layer L_i , a subset of the original components \mathcal{I}_i that preserves the network’s performance while reducing its size.

3.2. Method Overview

Our proposed method, Automatic Complementary Separation Pruning (ACSP), aims to automatically determine the

Algorithm 1 Automatic Complementary Separation Pruning

Input: Neural Network $F(D; W)$, Dataset $D = (X, Y)$

```

1: for each layer  $L_i$  in  $F(D; W)$  do
2:    $W_i \leftarrow$  extract weights from  $L_i$ 
3:    $N_i \leftarrow$  number of components in  $L_i$ 
4:    $A_i \leftarrow$  extract activations from  $L_i$  using  $D$ 
5:    $graph\_space \leftarrow$  construct graph space for  $L_i$ 
6:    $S \leftarrow \emptyset$  ▷ MSS Array
7:   for each  $k \in \{2, \dots, N_i\}$  do
8:     Apply  $k$ -Medoid to  $graph\_space$ 
9:      $S[k] \leftarrow$  Calculate MSS
10:  end for
11:   $k' \leftarrow$  apply Kneedle algorithm on  $S$ 
12:   $optimal\_components \leftarrow k'$  weighted components
13:  Prune all  $L_i$  components except  $optimal\_components$ 
14:  Fine-tune the model on  $D$ 
15: end for

```

size and composition of the smallest subset of components in each layer, without degrading the model’s performance.

For each layer L_i , we construct a graph space that encodes the separability of each component with respect to all pairs of classes in the dataset. Each component is evaluated based on its separation score for these class pairs. This information is encoded into a vector of size $1 \times (p \times p \times \binom{C}{2})$, representing the component’s position in the graph space of that layer. Further details on the construction of this graph space are provided in Sec. 3.3.1.

To determine the size and composition of the smallest subset of components for layer L_i , we assign a score to each potential subset size in the range $[2, N_i]$. Our method employs the principle of complementary selection, which selects components with diverse and complementary separability capabilities, minimizing redundancy among components with similar separability properties. To implement this, we use a clustering algorithm that selects components from different regions of the graph space, ensuring complementary separation capabilities. The quality of each subset size is evaluated using the Mean Simplified Silhouette (MSS) index [29], which provides a score for each tested subset size. Sec. 3.3.2 provides additional details on the selection and scoring process.

Finally, after scoring each subset size, we apply a kneefinding algorithm to identify the optimal subset size. The component subset corresponding to this size is then selected from the clustering process. Further details of the kneefinding process are in Sec. 3.4.1. At this stage, all components in the layer, apart from the identified subset, are pruned. Following this, a short fine-tuning process is conducted on a portion of the dataset to acclimate the remaining layers to the pruned layer, allowing them to adjust and optimize performance with the updated network structure. The full algorithm for this procedure is outlined in Algorithm 1.

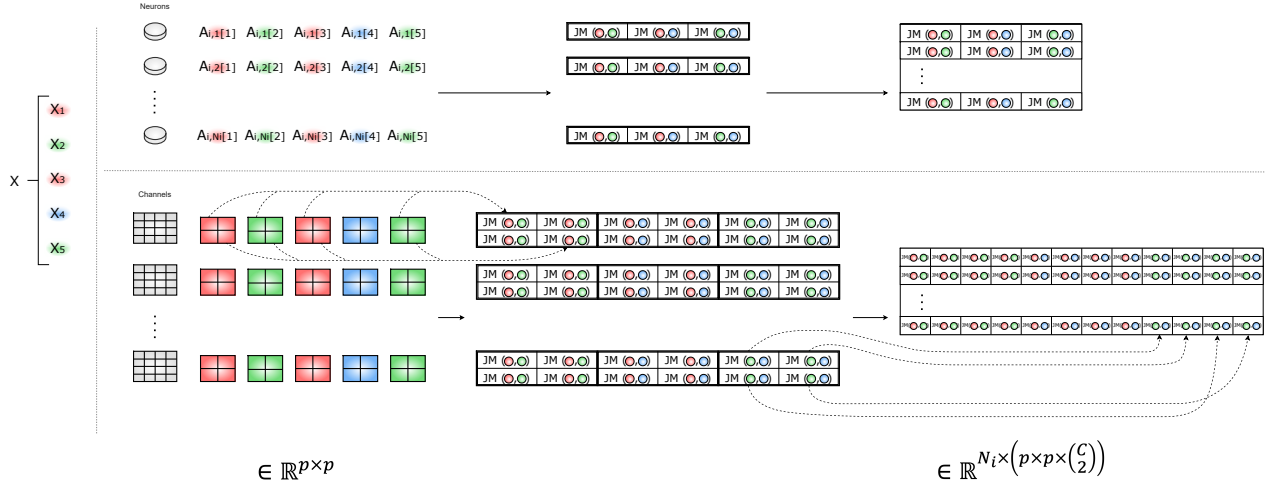


Figure 1. Building the separation matrix for a single layer, which defines the graph space: the upper part for a linear layer, and the lower for a convolutional layer. [I] A set of samples X , each sample x_i with a label (color). [II] Perform a forward pass to obtain activations for each sample. [III] Calculate a JM value for each component and class pair, forming a separability vector. [IV] Create the matrix representation, with each row representing a component’s separability, forming the graph space.

In the following sections, we describe the steps for pruning a single layer, i.e., how to select a subset of components to retain while pruning the rest. This process is applied iteratively to each layer in the network, starting from the first hidden layer to the last, excluding the input and output layers. By following this approach, the entire model is pruned layer by layer.

3.3. Graph Space Representation

3.3.1 Constructing the Graph Space

The objective of this step is to construct a graph space for a given layer L_i , that encodes the separability of its components \mathcal{I}_i across all class pairs (c, \tilde{c}) , where $1 \leq c, \tilde{c} \leq C$. For each component \mathcal{I}_i, j , the separability information is encoded to a vector of size $1 \times (p \times p \times \binom{C}{2})$, indicating its position in the graph space of layer L_i . The process of encoding the separability vector is performed differently for linear and convolutional layers. The process of creating the graph space is illustrated in Fig. 1.

Linear Layer. We begin by performing a forward pass of the dataset D through the network to extract activations from layer L_i . For each sample in X , we obtain N_i activation values, where each activation corresponds to a scalar value for every neuron \mathcal{I}_i, j in layer L_i . To quantify the separability of a neuron \mathcal{I}_i, j with respect to a pair of classes (c, \tilde{c}) , we compute the Jeffries-Matusita (JM) distance [53, 56] between the activation values $A_{i,j}$ obtained from samples labeled as class c and samples labeled as class \tilde{c} , with respect to neuron \mathcal{I}_i, j .

The JM distance between these two groups of activations

is calculated as:

$$JM_{i,j}(c, \tilde{c}) = 2 \left(1 - e^{-B_{i,j}(c, \tilde{c})} \right) \quad (1)$$

where the Bhattacharyya distance $B_{i,j}(c, \tilde{c})$ is given by:

$$B_{i,j}(c, \tilde{c}) = \frac{1}{8} \frac{(\mu_{i,j,c} - \mu_{i,j,\tilde{c}})^2}{\sigma_{i,j,c}^2 + \sigma_{i,j,\tilde{c}}^2} + \frac{1}{2} \ln \left(\frac{\sigma_{i,j,c}^2 + \sigma_{i,j,\tilde{c}}^2}{2\sigma_{i,j,c}\sigma_{i,j,\tilde{c}}} \right). \quad (2)$$

Here, $\mu_{i,j,c}$ and $\sigma_{i,j,c}^2$ represent the mean and variance of the activation values $A_{i,j}$ for class c , respectively, and similarly for class \tilde{c} . The JM distance serves as the separability score of neuron \mathcal{I}_i, j between the classes c and \tilde{c} .

The process is repeated for all neurons \mathcal{I}_i, j in layer L_i and for all class pairs (c, \tilde{c}) . The separability values for each component \mathcal{I}_i, j are encoded into a vector of size $1 \times (p \times p \times \binom{C}{2})$, where $p = 1$ for linear layers. The final matrix for layer L_i has dimensions $N_i \times (p \times p \times \binom{C}{2})$, where N_i is the number of neurons in the layer, and each row represents the ability of one neuron to separate between all class pairs.

Convolutional Layer. In convolutional layers, each sample t in X produces N_i activation maps from layer L_i , where each activation map $A_{i,j}[t]$ is a $p \times p$ matrix corresponding to a filter. To compute the separability of a channel \mathcal{I}_i, j between classes (c, \tilde{c}) , we extract the activation maps $A_{i,j}$ from samples labeled as classes c and \tilde{c} .

For each pixel in these maps, we calculate the JM distance between the pixel values from samples labeled as class c and samples labeled as class \tilde{c} , similar to the neuron-level computation in linear layers. After calculating separability for each pixel, the resulting $p \times p$ matrix is flattened

into a vector of size $1 \times (p \times p)$. This is done for all class pairs, yielding a separability vector of size $1 \times (p \times p \times \binom{C}{2})$ for each channel \mathcal{I}_i, j . The final matrix for layer L_i has dimensions $N_i \times (p \times p \times \binom{C}{2})$, where N_i is the number of channels in the layer, and each row represents the separation ability of a channel across all class pairs.

3.3.2 Graph Space Evaluation

As mentioned, our goal is to select components with complementary separation capabilities. At a graphical level, this translates into selecting components from diverse regions of the graph space to ensure the broadest coverage.

Consider three components \mathcal{I}_i, j , \mathcal{I}_i, k , and \mathcal{I}_i, l , each represented by their respective separation vectors in the graph space. Suppose the components \mathcal{I}_i, j and \mathcal{I}_i, k exhibit similar separation capabilities, while \mathcal{I}_i, l displays different separation capabilities. Graphically, this means that \mathcal{I}_i, j and \mathcal{I}_i, k are located near each other in the graph space, while \mathcal{I}_i, l is located in a more distant region. When selecting two components, we would prioritize selecting either \mathcal{I}_i, j or \mathcal{I}_i, k in combination with \mathcal{I}_i, l , thereby choosing components with complementary separation capabilities. Even if \mathcal{I}_i, j and \mathcal{I}_i, k have higher separation values than \mathcal{I}_i, l , their proximity in the graph space makes them less desirable as a pair. Instead, we aim to select one component from a different region, like \mathcal{I}_i, l , even if its separation value is lower, as this would yield a more diverse and complementary set of separation capabilities.

To achieve this complementary selection of components, we employ the k -Medoids [27] algorithm. This algorithm partitions the graph space into k clusters, with each cluster containing components with similar separation capabilities. After the clustering process, the medoids of the clusters are selected, representing the subset of components that provides the widest distribution of the graph space, thus satisfying the principle of complementary selection.

Since the optimal value of k can range from 2 to N_i , we must evaluate the quality of the clustering result to ensure that the selected components adequately cover the graph space. To assess this, we utilize the MSS index, which measures how well the medoids reflect the principle of wide distribution within the graph space.

Mean Simplified Silhouette

The Mean Simplified Silhouette (MSS) index [29] is used to evaluate clustering algorithms in the context of component selection, emphasizing diversity and full coverage of the graph space while minimizing redundancy. Traditional indices like the Silhouette [47] and Simplified Silhouette [22, 55], assess how closely a point is associated with its cluster or medoid, and how distinct it is from the nearest non-belongs cluster. However, these methods focus only

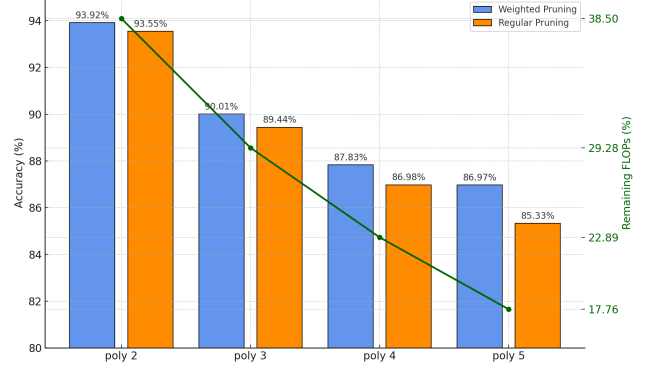


Figure 2. The effect of polynomial degree on the VGG-16 model on CIFAR-10 dataset. Higher polynomial degrees lead to fewer remaining FLOPs (%) but with a greater loss in accuracy.

on the nearest cluster, ignoring the broader layout of the graph space, which is essential for achieving complementary selection. MSS addresses this limitation by measuring the separation between a point and all other clusters, ensuring that the selected components are not only well-associated with their cluster but also widely spread across the graph space. This ensures that the chosen components complement each other and fully represent the space.

To compute the MSS index, for each point i , we define $a(i)$ as the distance between point i and the center of its assigned cluster C_h :

$$a(i) = d(i, C_h). \quad (3)$$

Next, $b(i)$ is defined as the average distance between point i and the centers of all other clusters C_l ($l \neq h$):

$$b(i) = \text{average}_{l \neq h} d(i, C_l). \quad (4)$$

The MSS score for point i is then:

$$mss(i) = 1 - \frac{a(i)}{b(i)}. \quad (5)$$

The MSS index is the average of these scores for all points.

3.4. Automatic Pruning

3.4.1 Optimal Component Size

To determine the minimal subset size of components that optimally preserves the model’s performance, we evaluate the quality of the solution provided for each subset size in the range $[2, N_i]$. For each size k in this range, we run the k -Medoids algorithm on the graph space and assess the resulting clusters using the MSS index.

After evaluating the MSS scores for all potential subset sizes, our goal is to pinpoint the point of diminishing returns, where further increases in subset size yield minimal

gains in coverage. We achieve this by applying the Kneedle algorithm [49], which detects the "knee point" in a data curve. This knee point indicates the transition from a steep improvement to a more gradual one, signaling the minimal size needed for optimal performance.

The Kneedle algorithm works by maximizing the curvature of a fitted curve, which represents the change in the MSS index across different subset sizes. Polynomial fitting is used to approximate this trend, with the degree of the polynomial influencing the flexibility of the model. A higher degree polynomial can introduce noise by fitting unnecessary local maxima, which may lead to earlier detection of the knee, i.e. a lower knee value, which will result in more aggressive pruning. On the other hand, a lower-degree polynomial may over-smooth the data, missing important changes in curvature.

The influence of polynomial degree on the pruning process is illustrated in Fig. 2, which shows the impact of different polynomial degrees on the accuracy of the VGG-16 model on the CIFAR-10 dataset and the corresponding remaining Floating Point Operations Per second (FLOPs). As the polynomial degree increases, we observe a gradual reduction in the remaining FLOPs, indicating more aggressive pruning. While this is desirable in terms of computational efficiency, it comes at the cost of model accuracy, which diminishes as the polynomial degree grows. This trend, which we illustrate solely to explain the mechanism, demonstrates that higher-degree polynomials can lead to excessive pruning, which significantly reduces model performance. Our method, however, is fully automatic and consistently uses a polynomial degree of 2 within the knee-finding algorithm to determine the optimal pruning point without manual adjustment. This choice of degree is validated in Sec. 4.5 through in-depth analyses across a broad range of architectures and datasets, showing that using a degree of 2 achieves extensive pruning with minimal impact on—or in some cases, an improvement of—model accuracy. This standardized, automatic approach eliminates the need for trial-and-error process in determining the pruning volume, ensuring that ACSP reliably and efficiently finds the optimal subset size and composition in each layer.

3.4.2 Optimal Component Composition

As mentioned, the Kneedle algorithm identifies the knee point in the MSS graph, which represents the optimal subset size for the components. The cluster space generated for the selected k value consists of k medoids, which reflect the broad structure of the graphical space, that captures the principle of complementary selection.

However, this selection process ignores the weights of the layer’s components. Weights are critical as they signify the importance of a component to the model’s performance.

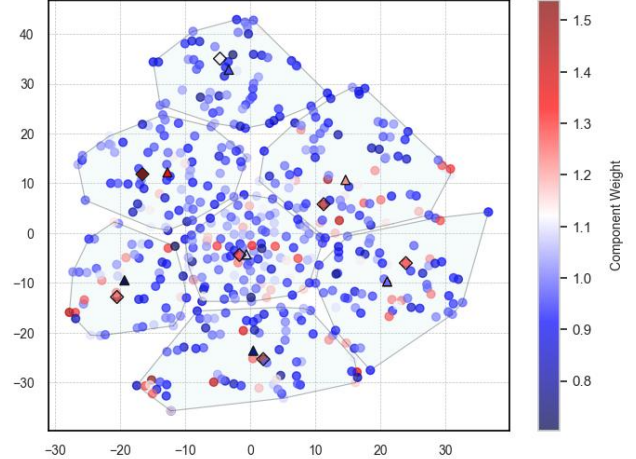


Figure 3. A 2-D representation of a ResNet-56 linear layer’s component space, where each point represents a component, colored by its weight. The space has 7 clusters, with medoids shown as triangles and the highest-weight components in each cluster shown as rhombuses.

Higher weights indicate components that contribute more significantly to the model’s predictive power. Neglecting weights in the selection process could lead to performance degradation after pruning.

To address this, we modify the selection by choosing the component with the largest weight from each cluster. This ensures that we not only maintain a wide distribution of the graph space, but also prioritize components with higher weights. By doing so, we preserve the model’s complementary separation capabilities while retaining the components most important for performance. Fig. 3 highlights the difference between these selection methods after reducing the graph space representation to 2-D using t-SNE technique [54]. Additionally, Fig. 2 and Tab. 3 demonstrate the effect of weighted pruning, where components are selected based on the highest weights in each cluster, resulting in higher accuracy compared to regular pruning, which selects the medoid as the representative component.

4. Experiments

4.1. Setup

We performed a comprehensive set of experiments on CIFAR-10, CIFAR-100 [28], and ImageNet-1K [5]. Our method was tested on a range of widely used architectures: VGG-16 and VGG-19 [50], DenseNet-40 [23], MobileNet-V2 [48], ResNet-50, and ResNet-56 [15].

We evaluated our method using three key metrics: **Base Accuracy** (pre-pruning), **Pruned Accuracy** (post-pruning), and **Speed Up**, measured as the ratio of the number of FLOPs before and after pruning. The results of our method

Model	Method	Base	Pruned	Δ Acc.	Speed Up
MobileNet-V2	Uniform [62]	94.47	94.17	-0.30	1.35×
	DCP [61]	94.47	94.69	+0.22	1.35×
	DMC [10]	94.23	94.49	+0.26	1.66×
	SCOP [52]	94.48	94.24	-0.24	1.67×
	ATO [57]	94.45	94.78	+0.33	1.84×
	SANP [11]	94.52	94.97	+0.45	1.85×
	ACSP	94.48	94.98	+0.50	1.93×
VGG-16	GAL [35]	93.96	90.78	-3.18	1.82×
	HRank [34]	93.96	93.43	-0.53	2.15×
	GCNP [25]	93.10	93.27	+0.17	2.34×
	CHIP [51]	93.96	93.86	-0.10	2.38×
	AOFP [7]	93.38	93.84	+0.46	2.52×
	APIB [12]	93.68	94.08	+0.40	2.50×
	ACSP	93.55	<u>93.92</u>	+0.37	2.59×
ResNet-56	Geometric [18]	93.59	93.26	-0.33	1.70×
	Polar [60]	93.80	93.82	+0.02	1.88×
	CP [30]	92.80	91.80	-1.00	2.00×
	AMC [19]	92.80	91.90	-0.90	2.00×
	HRank [34]	93.26	92.17	-1.09	2.00×
	SFP [17]	93.59	93.36	-0.23	2.11×
	DepGraph [9]	93.53	<u>93.77</u>	+0.24	2.11×
	ResRep [8]	93.71	93.71	+0.00	2.12×
	ACSP	93.69	93.82	+0.13	2.15×

Table 1. Pruning results on CIFAR-10. Best and second-best results are in bold and underlined, respectively, for each model.

presented in this section were obtained using a second-degree polynomial in the Kneedle algorithm, combined with weight-based component selection.

4.2. CIFAR-10 Results

For CIFAR-10, we tested our method on MobileNet-V2, VGG-16, and ResNet-56. Tab. 1 presents the results.

MobileNet-V2. Our method yields the highest post-pruning accuracy of 94.98% with a +0.5% accuracy gain, outperforming existing approaches such as SANP (+0.45% accuracy gain) and DMC (+0.26% accuracy gain). Notably, our method also provides the best speed-up, achieving a 1.93× improvement, making it the most effective both in accuracy retention and computational efficiency.

VGG-16. Although AOFP achieves the highest accuracy gain (+0.46%), our method performs almost as well with a +0.37% accuracy improvement, while delivering the highest speed-up at 2.59×. This positions our method as a well-rounded solution, balancing both accuracy and efficiency in the pruning process for VGG-16.

ResNet-56. Our method achieves an accuracy gain of +0.13%, which is lower than DepGraph’s +0.24% improvement. However, it provides the highest speed-up at 2.15×, demonstrating its strength in computational performance. DepGraph comes close with a 2.11× speed-up but slightly surpasses us in accuracy.

Model	Method	Base	Pruned	Δ Acc.	Speed Up
VGG-16	Polar [60]	73.83	<u>74.25</u>	+0.42	1.75×
	DLRFC [20]	73.54	74.09	<u>+0.55</u>	1.76×
	SCP [26]	73.51	73.86	+0.35	2.06×
	ACSP	73.70	74.31	+0.61	<u>2.01×</u>
VGG-19	NS [38]	73.26	<u>73.48</u>	+0.22	1.59×
	SCP [26]	72.56	72.99	<u>+0.43</u>	1.69×
	SOSP [43]	73.45	73.11	-0.34	<u>2.06×</u>
	ACSP	73.38	73.90	+0.62	2.11×
DenseNet-40	SOSP [43]	74.11	73.46	<u>-0.65</u>	1.42×
	SCP [26]	74.24	73.17	-1.07	1.86×
	NS [38]	74.64	74.28	-0.36	1.89×
	ACSP	74.30	<u>73.94</u>	-0.36	1.91×

Table 2. Pruning results on CIFAR-100. Best and second-best results are in bold and underlined, respectively, for each model.

4.3. CIFAR-100 Results

For CIFAR-100, we tested our method on VGG-16, VGG-19, and DenseNet-40. Tab. 2 presents the results.

VGG-16. Our method achieves the highest accuracy post-pruning (74.31%) with a notable +0.61% accuracy gain, surpassing other methods such as DLRFC (+0.55%) and PR (+0.42%). While SCP offers a slightly better speed-up (2.06×), our method closely follows with a 2.01× improvement, achieving a balance between accuracy and computational efficiency.

VGG-19. Our method again demonstrates superior performance, achieving the highest post-pruning accuracy (73.90%) with a +0.62% gain. While other methods like NS and SCP show smaller improvements, SOSP experiences a performance drop after pruning.

DenseNet-40. Our method provides a competitive performance with a minimal accuracy drop of −0.36%, matching NS in accuracy retention. In terms of speed-up, our method slightly edges out other approaches with a 1.91× improvement, making it the most efficient in this comparison.

4.4. ImageNet-1K Results

For ImageNet-1K, we tested our method on MobileNet-V2 and ResNet-50. Tab. 4 presents the results.

MobileNet-V2. Our method achieves an accuracy of 71.99% after pruning, with a modest but positive accuracy gain of +0.09%. Although SANP slightly outperforms us in accuracy gain (+0.14%), our method delivers the highest speed-up at 1.55×, making it more efficient in terms of computational improvement. Competing methods like MetaPruning and AMC show large accuracy drops.

ResNet-50. Our method demonstrates excellent performance, achieving a significant speed-up of 2.25× - the highest among all approaches. In terms of accuracy gain, our method is second to CCP (+0.83% gain) with a

Dataset	Model	Method	Base		Poly 2		Poly 3		Poly 4		Poly 5	
			Accuracy	FLOPs	Accuracy	FLOPs	Accuracy	FLOPs	Accuracy	FLOPs	Accuracy	FLOPs
CIFAR-10	MobileNet-V2	Regular	94.48	-	94.51	51.81	90.12	39.62	87.87	30.80	86.34	24.07
		Weighted			94.98		90.71		88.82		87.95	
	VGG-16	Regular	93.55	-	93.55	38.50	89.44	29.28	86.98	22.89	85.33	17.76
		Weighted			93.92		90.01		87.83		86.97	
	ResNet-56	Regular	93.69	-	93.41	46.51	89.28	35.40	86.93	27.66	85.03	23.50
		Weighted			93.82		90.21		87.97		86.89	
CIFAR-100	VGG-16	Regular	73.70	-	73.95	49.75	70.69	36.14	68.67	30.38	67.57	24.10
		Weighted			74.31		71.08		69.68		68.79	
	VGG-19	Regular	73.38	-	73.36	47.39	69.95	38.91	68.30	33.63	67.16	27.34
		Weighted			73.90		70.89		68.83		68.00	
	DenseNet-40	Regular	74.30	-	73.51	52.35	70.23	39.62	69.13	30.84	67.91	23.98
		Weighted			73.94		70.85		69.34		68.75	
ImageNet-1K	MobileNet-V2	Regular	71.90	-	71.83	64.51	68.46	49.33	66.51	38.63	65.54	32.09
		Weighted			71.99		69.19		67.34		66.41	
	ResNet-50	Regular	76.32	-	76.40	44.44	73.29	36.77	71.36	28.51	69.61	24.56
		Weighted			76.98		73.98		72.02		71.15	

Table 3. Performance comparison of accuracy and remaining FLOPs (%) across different polynomial approximation levels, using regular and weighted component selection methods.

+0.66% accuracy improvement. Other methods, such as CHIP and SMCP, also show competitive accuracy gains but fall short of our method’s computational efficiency.

Model	Method	Base	Pruned	Δ Acc.	Speed Up
MobileNet-V2	CC [33]	71.88	70.91	-0.97	1.39×
	Rand. Pruning [32]	71.91	70.90	-1.01	1.41×
	SANP [11]	71.91	72.05	+0.14	1.41×
	Uniform [62]	71.80	69.80	-2.00	1.43×
	AMC [19]	71.80	70.80	-1.00	1.43×
	MetaPruning [36]	72.00	71.80	-0.80	1.44×
	ACSP	71.90	<u>71.99</u>	<u>+0.09</u>	1.55×
ResNet-50	DECORE [1]	76.15	74.58	-1.57	1.73×
	HRank [34]	76.15	74.98	-1.17	1.77×
	CHIP [51]	76.15	76.30	+0.15	1.81×
	CCP [44]	76.15	76.98	+0.83	2.04×
	PaS [31]	76.65	76.70	+0.05	2.05×
	SMCP [24]	76.20	<u>76.80</u>	+0.60	2.15×
	JMDP [37]	76.60	76.00	-0.60	2.15×
	FPGM [18]	76.15	75.59	-0.56	2.15×
	ResRep [8]	76.15	76.15	+0.00	2.20×
	ACSP	76.32	76.98	<u>+0.66</u>	2.25×

Table 4. Pruning results on ImageNet-1K. Best and second-best results are in bold and underlined, respectively, for each model.

4.5. Analysis of Our Method

Tab. 3 illustrates a comparison across various datasets and architectures to explain the rationale behind choosing a polynomial degree of 2 within the knee-finding algorithm. This comparison is solely provided to illustrate how different polynomial degrees influence the balance between model accuracy and pruning volume, guiding our choice of degree 2 to achieve this optimal balance. It is important to note that the knee-point polynomial degree is not a component of the method itself but rather an external decision that

supports ACSP’s effectiveness. The table further includes two selection methods: the “Regular” method, which selects the k medoids identified at the end of clustering, and the “Weighted” method, which selects the k components with the highest weights, one from each cluster.

Method. The weighted method consistently outperforms the regular method across all combinations of datasets, architectures, and polynomial degrees. This highlights the significance of incorporating network weights in the component selection process.

Polynomial degree. As the polynomial degree increases, the number of remaining FLOPs (%) decreases, reflecting more aggressive pruning. The polynomial degree influences the knee value the Kneedle algorithm returns: higher degrees result in smaller knee values, leading to fewer components remaining after pruning. However, higher polynomial degrees also result in greater compromises in the model’s accuracy after pruning. As explained in Sec. 3.4.1, a polynomial degree of 2 applies maximum pruning while preserving, or improving in some cases, the performance of the full neural architecture, and therefore defines the automatic selection pruning point of the method.

5. Conclusion

We introduced Automatic Complementary Separation Pruning (ACSP), an automated method that combines structured and activation-based pruning to reduce network complexity while preserving performance. ACSP selects components with complementary capabilities, eliminating the need for manually defining the pruning volume and reducing redundancy. Experiments show that ACSP consistently reduces

computational costs while maintaining high accuracy across a variety of network models. These results demonstrate its effectiveness in optimizing neural networks for real-world classification applications. Since ACSP relies on class separability to construct its graph space, adapting it to unsupervised or semi-supervised settings presents a challenge. Future work could explore extending ACSP to unlabeled data, enabling it to support a broader range of applications.

References

- [1] Manoj Alwani, Yang Wang, and Vashisht Madhavan. Decore: Deep compression with reinforcement learning. In *Proceedings of the IEEE/CVF Conference on Computer Vision and Pattern Recognition*, pages 12349–12359, 2022. 8
- [2] Sajid Anwar, Kyuyeon Hwang, and Wonyong Sung. Structured pruning of deep convolutional neural networks. *ACM Journal on Emerging Technologies in Computing Systems (JETC)*, 13(3):1–18, 2017. 1
- [3] Arash Ardakani, Carlo Condo, and Warren J Gross. Activation pruning of deep convolutional neural networks. In *2017 IEEE Global Conference on Signal and Information Processing (GlobalSIP)*, pages 1325–1329. IEEE, 2017. 1
- [4] Davis Blalock, Jose Javier Gonzalez Ortiz, Jonathan Frankle, and John Guttag. What is the state of neural network pruning? *Proceedings of machine learning and systems*, 2:129–146, 2020. 2
- [5] Jia Deng, Wei Dong, Richard Socher, Li-Jia Li, Kai Li, and Li Fei-Fei. Imagenet: A large-scale hierarchical image database. In *Proceedings of the IEEE Conference on Computer Vision and Pattern Recognition (CVPR)*, pages 248–255. IEEE, 2009. doi: 10.1109/CVPR.2009.5206848. 6
- [6] Emily L Denton, Wojciech Zaremba, Joan Bruna, Yann LeCun, and Rob Fergus. Exploiting linear structure within convolutional networks for efficient evaluation. *Advances in neural information processing systems*, 27, 2014. 1
- [7] Xiaohan Ding, Guiguang Ding, Yuchen Guo, Jungong Han, and Chenggang Yan. Approximated oracle filter pruning for destructive cnn width optimization. In *International Conference on Machine Learning*, pages 1607–1616. PMLR, 2019. 7
- [8] Xiaohan Ding, Tianxiang Hao, Jianchao Tan, Ji Liu, Jungong Han, Yuchen Guo, and Guiguang Ding. Resrep: Lossless cnn pruning via decoupling remembering and forgetting. In *Proceedings of the IEEE/CVF international conference on computer vision*, pages 4510–4520, 2021. 7, 8
- [9] Gongfan Fang, Xinyin Ma, Mingli Song, Michael Bi Mi, and Xinchao Wang. Depgraph: Towards any structural pruning. In *Proceedings of the IEEE/CVF conference on computer vision and pattern recognition*, pages 16091–16101, 2023. 2, 7
- [10] Shangqian Gao, Feihu Huang, Jian Pei, and Heng Huang. Discrete model compression with resource constraint for deep neural networks. In *Proceedings of the IEEE/CVF conference on computer vision and pattern recognition*, pages 1899–1908, 2020. 7
- [11] Shangqian Gao, Zeyu Zhang, Yanfu Zhang, Feihu Huang, and Heng Huang. Structural alignment for network pruning through partial regularization. In *Proceedings of the IEEE/CVF International Conference on Computer Vision*, pages 17402–17412, 2023. 2, 7, 8
- [12] Song Guo, Lei Zhang, Xiwu Zheng, Yan Wang, Yuchao Li, Fei Chao, Chenglin Wu, Shengchuan Zhang, and Rongrong Ji. Automatic network pruning via hilbert-schmidt independence criterion lasso under information bottleneck principle. In *Proceedings of the IEEE/CVF international conference on computer vision*, pages 17458–17469, 2023. 7
- [13] Song Han, Huizi Mao, and William J Dally. Deep compression: Compressing deep neural networks with pruning, trained quantization and huffman coding. *arXiv preprint arXiv:1510.00149*, 2015. 1
- [14] Song Han, Jeff Pool, John Tran, and William Dally. Learning both weights and connections for efficient neural network. *Advances in neural information processing systems*, 28, 2015. 1
- [15] Kaiming He, Xiangyu Zhang, Shaoqing Ren, and Jian Sun. Deep residual learning for image recognition. In *Proceedings of the IEEE conference on computer vision and pattern recognition (CVPR)*, pages 770–778, 2016. doi: 10.1109/CVPR.2016.90. 6
- [16] Yang He and Lingao Xiao. Structured pruning for deep convolutional neural networks: A survey. *IEEE transactions on pattern analysis and machine intelligence*, 2023. 1
- [17] Yang He, Guoliang Kang, Xuanyi Dong, Yanwei Fu, and Yi Yang. Soft filter pruning for accelerating deep convolutional neural networks. *arXiv preprint arXiv:1808.06866*, 2018. 7
- [18] Yang He, Ping Liu, Ziwei Wang, Zhilan Hu, and Yi Yang. Filter pruning via geometric median for deep convolutional neural networks acceleration. In *Proceedings of the IEEE/CVF conference on computer vision and pattern recognition*, pages 4340–4349, 2019. 7, 8
- [19] Yihui He, Ji Lin, Zhijian Liu, Hanrui Wang, Li-Jia Li, and Song Han. Amc: Automl for model compression and acceleration on mobile devices. In *Proceedings of the European conference on computer vision (ECCV)*, pages 784–800, 2018. 7, 8

- [20] Zhiqiang He, Yaguan Qian, Yuqi Wang, Bin Wang, Xiaohui Guan, Zhaoquan Gu, Xiang Ling, Shaoning Zeng, Haijiang Wang, and Wujie Zhou. Filter pruning via feature discrimination in deep neural networks. In *European conference on computer vision*, pages 245–261. Springer, 2022. 7
- [21] Geoffrey Hinton, Oriol Vinyals, and Jeff Dean. Distilling the knowledge in a neural network, 2015. URL <https://arxiv.org/abs/1503.02531>. 1
- [22] Eduardo R Hruschka, Ricardo JGB Campello, and Leandro N De Castro. Evolving clusters in gene-expression data. *Information Sciences*, 176(13):1898–1927, 2006. 5
- [23] Gao Huang, Zhuang Liu, Laurens Van Der Maaten, and Kilian Q Weinberger. Densely connected convolutional networks. In *Proceedings of the IEEE conference on computer vision and pattern recognition (CVPR)*, pages 4700–4708, 2017. doi: 10.1109/CVPR.2017.243. 6
- [24] Ryan Humble, Maying Shen, Jorge Albericio Latorre, Eric Darve, and Jose Alvarez. Soft masking for cost-constrained channel pruning. In *European Conference on Computer Vision*, pages 641–657. Springer, 2022. 8
- [25] Di Jiang, Yuan Cao, and Qiang Yang. On the channel pruning using graph convolution network for convolutional neural network acceleration. In *IJCAI*, pages 3107–3113, 2022. 7
- [26] Minsoo Kang and Bohyung Han. Operation-aware soft channel pruning using differentiable masks. In *International conference on machine learning*, pages 5122–5131. PMLR, 2020. 7
- [27] Leonard Kaufman and Peter J Rousseeuw. *Finding groups in data: an introduction to cluster analysis*. John Wiley & Sons, 2009. 5
- [28] Alex Krizhevsky. Learning multiple layers of features from tiny images. Technical report, University of Toronto, 2009. URL <https://www.cs.toronto.edu/~kriz/learning-features-2009-TR.pdf>. 6
- [29] David Levin and Gonen Singer. Gb-afs: graph-based automatic feature selection for multi-class classification via mean simplified silhouette. *Journal of Big Data*, 11(1):79, 2024. 2, 3, 5
- [30] Hao Li, Asim Kadav, Igor Durdanovic, Hanan Samet, and Hans Peter Graf. Pruning filters for efficient convnets, 2017. URL <https://arxiv.org/abs/1608.08710>. 1, 7
- [31] Yanyu Li, Pu Zhao, Geng Yuan, Xue Lin, Yanzhi Wang, and Xin Chen. Pruning-as-search: Efficient neural architecture search via channel pruning and structural reparameterization. *arXiv preprint arXiv:2206.01198*, 2022. 8
- [32] Yawei Li, Kamil Adamczewski, Wen Li, Shuhang Gu, Radu Timofte, and Luc Van Gool. Revisiting random channel pruning for neural network compression. In *Proceedings of the IEEE/CVF conference on computer vision and pattern recognition*, pages 191–201, 2022. 2, 8
- [33] Yuchao Li, Shaohui Lin, Jianzhuang Liu, Qixiang Ye, Mengdi Wang, Fei Chao, Fan Yang, Jincheng Ma, Qi Tian, and Rongrong Ji. Towards compact cnns via collaborative compression. In *Proceedings of the IEEE/CVF Conference on Computer Vision and Pattern Recognition*, pages 6438–6447, 2021. 8
- [34] Mingbao Lin, Rongrong Ji, Yan Wang, Yichen Zhang, Baochang Zhang, Yonghong Tian, and Ling Shao. Hrank: Filter pruning using high-rank feature map. In *Proceedings of the IEEE/CVF conference on computer vision and pattern recognition*, pages 1529–1538, 2020. 7, 8
- [35] Shaohui Lin, Rongrong Ji, Chenqian Yan, Baochang Zhang, Liujuan Cao, Qixiang Ye, Feiyue Huang, and David Doermann. Towards optimal structured cnn pruning via generative adversarial learning. In *Proceedings of the IEEE/CVF conference on computer vision and pattern recognition*, pages 2790–2799, 2019. 7
- [36] Zechun Liu, Haoyuan Mu, Xiangyu Zhang, Zichao Guo, Xin Yang, Kwang-Ting Cheng, and Jian Sun. Metapruning: Meta learning for automatic neural network channel pruning. In *Proceedings of the IEEE/CVF international conference on computer vision*, pages 3296–3305, 2019. 8
- [37] Zechun Liu, Xiangyu Zhang, Zhiqiang Shen, Yichen Wei, Kwang-Ting Cheng, and Jian Sun. Joint multi-dimension pruning via numerical gradient update. *IEEE Transactions on Image Processing*, 30:8034–8045, 2021. 8
- [38] Zhuang Liu, Jianguo Li, Zhiqiang Shen, Gao Huang, Shoumeng Yan, and Changshui Zhang. Learning efficient convolutional networks through network slimming. In *Proceedings of the IEEE international conference on computer vision*, pages 2736–2744, 2017. 3, 7
- [39] Zhuang Liu, Mingjie Sun, Tinghui Zhou, Gao Huang, and Trevor Darrell. Rethinking the value of network pruning. *arXiv preprint arXiv:1810.05270*, 2018. 1
- [40] Jian-Hao Luo, Jianxin Wu, and Weiyao Lin. Thinet: A filter level pruning method for deep neural network compression. In *Proceedings of the IEEE international conference on computer vision*, pages 5058–5066, 2017. 3
- [41] Shervin Minaee, Yuri Boykov, Fatih Porikli, Antonio Plaza, Nasser Kehtarnavaz, and Demetri Terzopoulos. Image segmentation using deep learning: A survey.

- IEEE transactions on pattern analysis and machine intelligence*, 44(7):3523–3542, 2021. 1
- [42] Feiping Nie, Xiaoqian Wang, Michael Jordan, and Heng Huang. The constrained laplacian rank algorithm for graph-based clustering. In *Proceedings of the AAAI conference on artificial intelligence*, volume 30, 2016. 2
- [43] Manuel Nonnenmacher, Thomas Pfeil, Ingo Steinwart, and David Reeb. Sosp: Efficiently capturing global correlations by second-order structured pruning. *arXiv preprint arXiv:2110.11395*, 2021. 7
- [44] Hanyu Peng, Jiaxiang Wu, Shifeng Chen, and Junzhou Huang. Collaborative channel pruning for deep networks. In *International conference on machine learning*, pages 5113–5122. PMLR, 2019. 8
- [45] Mohammad Rastegari, Vicente Ordonez, Joseph Redmon, and Ali Farhadi. Xnor-net: Imagenet classification using binary convolutional neural networks. In *European conference on computer vision*, pages 525–542. Springer, 2016. 1
- [46] J Redmon. You only look once: Unified, real-time object detection. In *Proceedings of the IEEE conference on computer vision and pattern recognition*, 2016. 1
- [47] Peter J Rousseeuw. Silhouettes: a graphical aid to the interpretation and validation of cluster analysis. *Journal of computational and applied mathematics*, 20: 53–65, 1987. 5
- [48] Mark Sandler, Andrew Howard, Menglong Zhu, Andrey Zhmoginov, and Liang-Chieh Chen. Mobilenetv2: Inverted residuals and linear bottlenecks. In *Proceedings of the IEEE conference on computer vision and pattern recognition*, pages 4510–4520, 2018. 6
- [49] Ville Satopaa, Jeannie Albrecht, David Irwin, and Barath Raghavan. Finding a” kneedle” in a haystack: Detecting knee points in system behavior. In *2011 31st international conference on distributed computing systems workshops*, pages 166–171. IEEE, 2011. 6
- [50] Karen Simonyan and Andrew Zisserman. Very deep convolutional networks for large-scale image recognition. *arXiv preprint arXiv:1409.1556*, 2014. URL <https://arxiv.org/abs/1409.1556>. 6
- [51] Yang Sui, Miao Yin, Yi Xie, Huy Phan, Saman Aliari Zonouz, and Bo Yuan. Chip: Channel independence-based pruning for compact neural networks. *Advances in Neural Information Processing Systems*, 34:24604–24616, 2021. 7, 8
- [52] Yehui Tang, Yunhe Wang, Yixing Xu, Dacheng Tao, Chunjing Xu, Chao Xu, and Chang Xu. Scop: Scientific control for reliable neural network pruning. *Advances in Neural Information Processing Systems*, 33: 10936–10947, 2020. 2, 7
- [53] Valentyn A Tolpekin and Alfred Stein. Quantification of the effects of land-cover-class spectral separability on the accuracy of markov-random-field-based super-resolution mapping. *IEEE transactions on geoscience and remote sensing*, 47(9):3283–3297, 2009. 4
- [54] Laurens Van der Maaten and Geoffrey Hinton. Visualizing data using t-sne. *Journal of machine learning research*, 9(11), 2008. 6
- [55] Fei Wang, Hector-Hugo Franco-Penya, John D Kelleher, John Pugh, and Robert Ross. An analysis of the application of simplified silhouette to the evaluation of k-means clustering validity. In *Machine Learning and Data Mining in Pattern Recognition: 13th International Conference, MLDM 2017, New York, NY, USA, July 15-20, 2017, Proceedings 13*, pages 291–305. Springer, 2017. 5
- [56] Yongji Wang, Qingwen Qi, and Ying Liu. Unsupervised segmentation evaluation using area-weighted variance and jeffries-matusita distance for remote sensing images. *Remote Sensing*, 10(8):1193, 2018. 4
- [57] Xidong Wu, Shangqian Gao, Zeyu Zhang, Zhenzhen Li, Runxue Bao, Yanfu Zhang, Xiaoqian Wang, and Heng Huang. Auto-train-once: Controller network guided automatic network pruning from scratch. In *Proceedings of the IEEE/CVF Conference on Computer Vision and Pattern Recognition*, pages 16163–16173, 2024. 7
- [58] Xia Xiao, Zigeng Wang, and Sanguthevar Rajasekaran. Autoprune: Automatic network pruning by regularizing auxiliary parameters. *Advances in neural information processing systems*, 32, 2019. 2
- [59] Haifeng Zhao, Qi Li, Zheng Wang, and Feiping Nie. Joint adaptive graph learning and discriminative analysis for unsupervised feature selection. *Cognitive Computation*, 14(3):1211–1221, 2022. 2
- [60] Tao Zhuang, Zhixuan Zhang, Yuheng Huang, Xiaoyi Zeng, Kai Shuang, and Xiang Li. Neuron-level structured pruning using polarization regularizer. *Advances in neural information processing systems*, 33:9865–9877, 2020. 7
- [61] Zhuangwei Zhuang, Minghui Tan, Bohan Zhuang, Jing Liu, Yong Guo, Qingyao Wu, Junzhou Huang, and Jinhui Zhu. Discrimination-aware channel pruning for deep neural networks. *Advances in neural information processing systems*, 31, 2018. 3, 7
- [62] Zhuangwei Zhuang, Minghui Tan, Bohan Zhuang, Jing Liu, Yong Guo, Qingyao Wu, Junzhou Huang, and Jinhui Zhu. Discrimination-aware channel pruning for deep neural networks, 2019. URL <https://arxiv.org/abs/1810.11809>. 7, 8